AIMS Energy, 8(5): 771–782.
DOI: 10.3934/energy.2020.5.771
Received: 21 May 2020
Accepted: 12 August 2020
Published: 25 August 2020

http://www.aimspress.com/journal/energy

Research article

Enhancing the vanadium redox flow battery efficiency by adjusting the electrode configuration

Mohammed A. Al-Yasiri*

Department of Mechanical Engineering, Wasit University, Kut, Iraq

* **Correspondence:** Email: maapbd@uowasit.edu.iq; Tel: +9647818331394.

Abstract: The vanadium redox flow battery (VRFB) is being investigated as one of the promising candidates for large-scale energy storage systems. In the present work, the role of electrode shape on a single VRFB cell performance has been studied through a 3D numerical model. The model accounts for the coupling between electrochemistry and fluid mechanic physics. Seven cases of electrode configurations at the same volume size (10 cm^3) have been simulated to investigate the overall battery performance. Results from the simulation show that the configuration (case 7) has the best battery efficiency, while the worse one is (case 4) under the same operating conditions, e.g., 71.72% and 63.82%, respectively. Also, the ratio of output to input power for (case 7) is 0.72, while 0.63 for (case 4). In addition, there is an optimal flow rate for each case to get maximum battery efficiency, which means a balance between electrochemical reactions and pumping losses is required. Overall, adopting a thicker electrode (cases 2, 3 and 4) results in lower battery performance due to the poor voltage responses. One feature of the introduced model is its capability to predict the performance of most flow batteries cell configurations.

Keywords: charging/discharging; numerical model; VRFB; electrode shape; battery efficiency

1. Introduction

Currently, burning the fossil fuel such as oil, coal, and gas is the major source of electrical output generation. This non-renewable source is limited with a lot of negative aspects in terms of environmental damage such as CO_2 production and other greenhouses gases that cause global warming. In order to combat global warming, many countries have begun phasing out energy production based on fossil fuels in order to reduce the amount of greenhouse gasses produced. This

has prompted researchers with an opportunity to develop 'clean' renewable energy resources such as wind, sun, wave, and tides to meet the increasing energy demand and to replace the current technology based on fossil fuels [1]. One slight downfall of these sources is the dependence on variable factors such as the wind speed and sunlight, i.e., weather, which cause fluctuations in energy output. [2,3]. Energy storage, therefore, is a common solution to supply continuous power and to anticipate an integration into the electric grid [4]. Flow batteries (FB) are the most common stationary electrochemical energy storage devices that store chemical energy and produce electricity by a redox reaction between ion species dissolved in electrolytes. Flow batteries have many desirable characteristics such as power and energy independency, long cycles of charge and discharge, and size control flexibility [5]. In addition to the desirable characteristics of (FB), VRFB utilizes same electrolyte and catholyte in both sides of the cell that can eliminate the contamination due to electrolyte crossover through the membrane, which reducing the effect of battery degradation [6–13].

Recently, some research has been focused numerically and/or experimentally on different cells of VRFBs by considering the impact of flow field, electrode and membrane materials, and types of electrolyte solutions and concentrations under various operating conditions at the aim of battery performance enhancement. Different types of flow channels have been experimentally performed to investigate their impact on the VRFB cell performance. The results showed that the cell with serpentine configuration has better performance among them in terms of voltage responses and pressure losses [14]. An experimental study of a new developed cell structure has been achieved in [15], which was introduced to overcome the issues of using conventional graphite, which are the weakness structure and electrolyte leakage by using polyvinyl chloride (PVC) sheets. The new structure showed many advantages such as the easiness of cell assembly and the low cost and weight of cell components. In Ref. [16], an important unresolved problems has been presented such as the way of designing the flow channel cross section, determining its length, and investigating its impact on the distribution of pressure losses in both electrodes. This was implemented through a verified 3D model to determine the voltage response, pressure losses, pumping power, and finally, the overall battery performance. It was found that channel height is an important geometric parameter that determines battery performance, rather than channel length. Also, a numerical and experimental study of a parallel flow field design has been conducted to predict the VRFB performance under various species concentrations [17], and the results from the numerical model and experiment work were in a good agreement. Another numerical study has been conducted to study the sensitivity of changing multi- input parameters on output response voltage for a single cell VRFB under various loading conditions [18], and it has been found that some input parameters had an impact on response voltage while others were not. Also, a polarization study has been conducted to investigate the VRFB performance for two types of cells: without flow field and flow field (serpentine pattern), and the results showed that the ohmic losses were dominant compared to polarization and activation losses for the cell with flow field, i.e., serpentine pattern [19]. An interdigitated flow channel configuration has been performed numerically through a 3D model of VRFB [20]. The distribution of pressure drops, vanadium concentrations, and current density was examined under two inlet structures of flow rates: single and multi-inlet structures.

Most relevant research on the literature, however, has focused on different aspects to improve the overall battery efficiency such as: the types of electrode and membrane materials, the concentration of vanadium solution, and various types of channel configurations, including serpentine, interdigital, parallel, and spiral. However, according to the author knowledge, there is no evidence that the current work about studying the role of different electrode configurations at same volume size on battery performance has been studied and reported in the literature. In this paper, the model represents a guidance for future VRFB designs to better understand the behavior of battery performance. Different case studies (7 cases) of electrode configurations at the same volume size have been performed in order to figure out their impact on output voltage response, pumping power losses, and finally the overall battery performance; and to determine the best option among them. The findings provide some insights for the optimization of electrodes in redox flow batteries as discussed below.

2. Model development

2.1. Geometric model building

Normally, a single electrochemical cell of VRFB contains a pair of electrodes (cathode and anode), ion-exchange membrane, and vanadium species stored in external tanks, as depicted in Figure 1a. In this study, a simplified 3D model of single cell VRFB is built to save computational time and memory space. The model includes porous electrodes for anode and cathode as depicted in Figure 1b, and an ion exchange membrane to separate the two half-cells. Seven designs of electrode configurations at the same volume size (10 cm^3), but at different electrode heights (H_{el}) and widths (W_{el}) are considered in this model. The dimensions of each case are listed in Table 1.

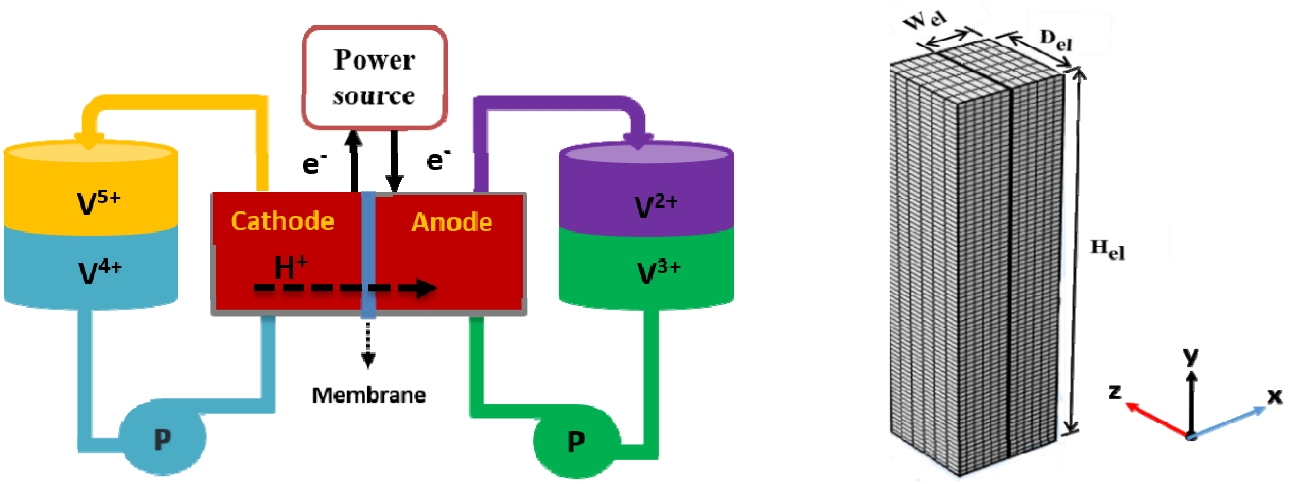

(a) (b)

Figure 1. (a) Simple diagram of a single VRFB during charge process, (b) 3D simulated electrode.

Table 1. Dimensions of seven cells for VRFB models.

Electrode dimension (cm)	Seven different cases of electrode configuration						
	Case 1	Case 2	Case 3	Case 4	Case 5	Case 6	Case 7
H_{el}	4	3.5	3	2	4.5	5	6
W_{el}	3	3	3	3	3	3	3
D_{el}	0.83	0.95	1.11	1.66	0.74	0.66	0.55

2.2. Model formulation

A 3-D steady state and isothermal VRFB model is considered in this work by using COMSOL software. More details regarding this model including assumptions: governing equations; boundary and initial conditions; and tables about the applied values of the kinetic, electrolyte, porous electrode properties, source/sink terms, and operating conditions can be found in our previously developed study [16]. Only three domains are taken into account in the current simulation (i.e., anode, membrane, and cathode) without considering the flow field part, i.e., no channels. A brief description of the main governing equations is formulated, as follows:

To develop the VRFB model for each domain, some assumptions are considered, as follows:

The motion of a charged chemical species in a fluid medium was described by Nernst-Plank [20]:

$$\overrightarrow{N_{i,e}} = -D_i^{eff}\,\nabla C_{i,e} - Z_i\,M_{i,e}\,C_{i,e}F\,\nabla \emptyset_{l,e} + \overrightarrow{u_l}\,C_{i,e} \quad (1)$$

where $\vec{N}_{i,e}$, D_i^{eff}, $C_{i,e}$, Z_i, $M_{i,e}$, F, $\emptyset_{l,e}$, $\overrightarrow{u_l}$ are the flux of the charged species (species of i) in the electrolyte (represented by subscript e), the effective diffusion coefficient, the species concentration, the valence for species i, the ionic (liquid) mobility, Faraday constant, the ionic potential, and the velocity of the electrolyte, respectively.

The species transport, electrochemical reactions, and current in the electrode domain are coupled through the conservation of charge [21]:

$$\nabla \cdot \overrightarrow{j_l} = -\nabla \cdot \overrightarrow{j_s} = I \quad (2)$$

where I is the reaction current density. $\overrightarrow{j_l}$ and $\overrightarrow{j_s}$ denote the total liquid and solid current density in both electrodes, respectively. Also, to predict accurate prediction of the cell potential without using a fitting voltage value, the Donnan potential across the membrane is accounted.

2.3. Simulated case studies

In this study, simulations are performed for different seven electrode configurations with same electrode volume size (10 cm^3). All cases are simulated at same operating conditions during charging/discharging processes, at the most utilized ones in literature, which include wide range of current densities (300 A/m^2, 600 A/m^2, and 900 A/m^2) and volumetric flow rates (3 ml/min, 10 ml/min, 40 ml/min, 90 ml/min, 160 ml/min, and 300 ml/min) at a range of SOCs (state of charges). In these simulations, the electrode dimensions for each case are listed in Table 1. Two termination conditions are applied in the charge and discharge processes. During charging process, the VRFB is charged from (SOC = 0.15 to 0.95 unless it reaches the cutoff voltage 1.7 V), while from (SOC = 0.95 to 0.1

unless it reaches the cutoff voltage 0.95 V) during discharging process. However, at low flow rate and high current density conditions, those termination conditions are not satisfied as it will be seen in Figure 2 in the next section.

3. Results and discussion

3.1. Voltage response under various operating conditions

It is necessary to balance the flow rate amount in VRFB operation so that the capacity can be increased. The lack in flow rate leads to reduce capacity utilization of electrolyte, while the abundance of it results in high pumping power losses and leakage issues, and accordingly, the overall system efficiency is reduced. In the plots of Figure 2, the left directed arrow refers to the left and bottom axes for voltage response against SOC during the charge process, whereas the right directed arrow refers to the right and top axes for voltage response against SOC during the discharge process. Figure 2a,b show the charge/discharge curves for range of flow rates (3, 10, 40, 90, 160, 300 ml/min) to the cell (case 1) at 30 and 90 mA/cm^2 current densities, respectively. It is clear that as the flow rate increases, the SOC during charge/discharge processes increases too due to the enhancement of vanadium ion utilization, which means the battery can store more energy, i.e., it has more capacity. The effect of flow rate becomes more significant as the current density increases, as shown in Figure 2b, due to the fact that more consumption of supplied vanadium ions takes place at high applied current density, which requires additional flow rate to improve the cell performance [22]. Figure 2c,d show the charge/discharge curves for range of current densities (30, 60, 90 mA/cm^2) at 3 and 300 ml/min, respectively. It is, also, shown that increasing the current density at constant volumetric flow rate leads to larger ohmic drop which, in turn, results in a quick jump in cell voltage through charging and lower initiated cell voltage through discharging processes. In some instances, the termination conditions are not satisfied as stated above. For instance, at low flow rate (3 ml/min in Figure 2b), the terminal condition during charge process is SOC = 0.73 instead of 0.95, and it is 0.275 instead of 0.1 during discharge process. This can be attributed to the (high concentration polarization) as a result of the lack of supplied amount of vanadium species to the electrode surface. The insufficient amount of provided electrolyte can make a quick raise in voltage (to reach 1.7 V at SOC < 0.95) and a quick drop in voltage (to reach 0.95 V at SOC > 0.1) during charging and discharging, respectively. Also, this effect can be noticed more clearly when high current density condition is applied, as shown in Figures 2c and 3b due to the same reason (concentration polarization).

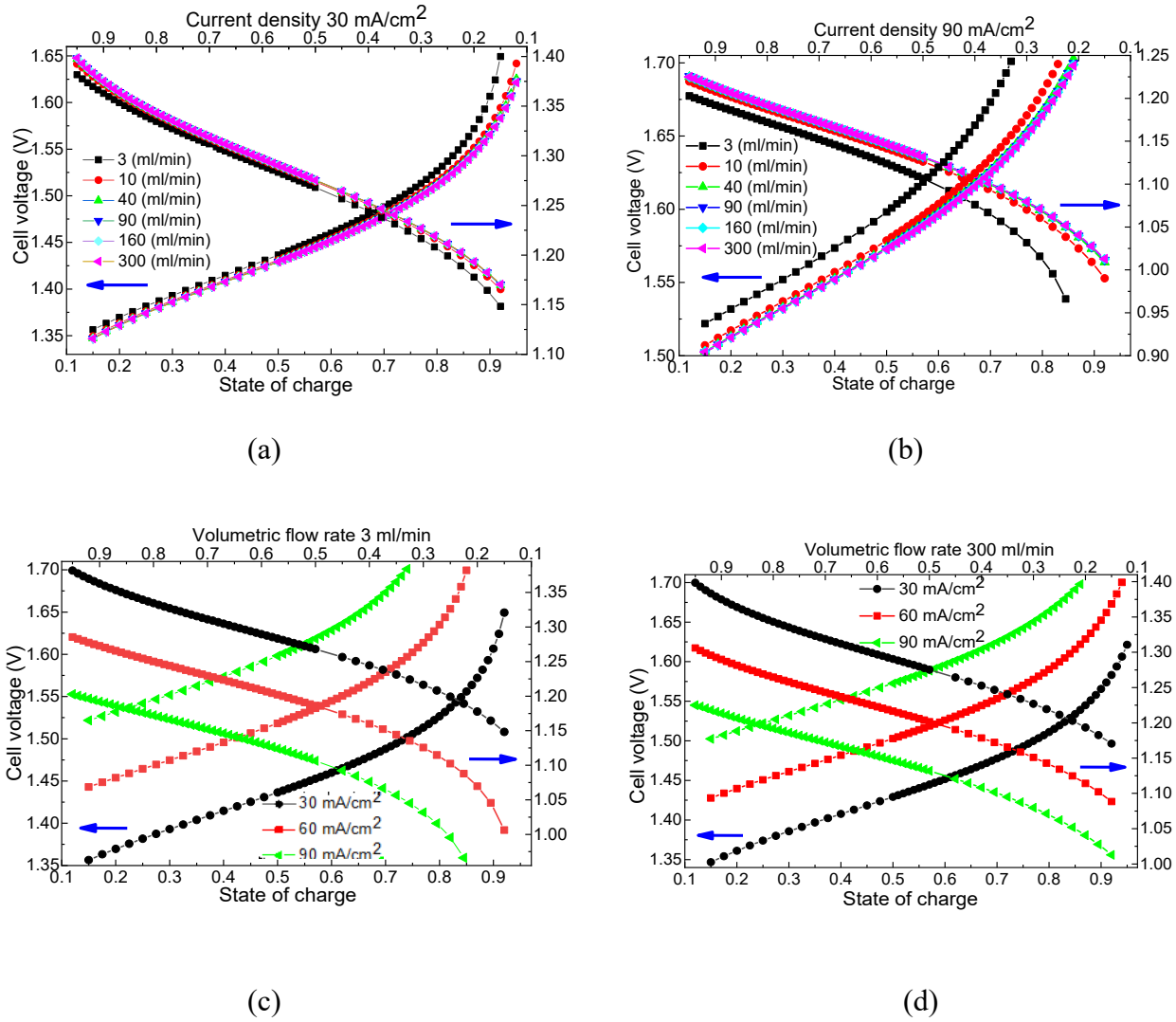

Figure 2. The voltage response in a charge/discharge processes at range of volumetric flow rates and current densities: (a) at current density 30 mA/cm^2, (b) at current density 90 mA/cm^2, (c) at flow rate 3 ml/min, (d) at flow rate 300 ml/min.

3.2. Voltage response at different cell configurations

The cell shape impact on discharge voltage behavior has been shown in Figure 3a,b for the conditions (30 mA/cm^2 and 90 mA/cm^2) at same flow rate of 300 ml/min, respectively. The enhancement in the discharge voltage for the cell (case 7) becomes more significant at high current density (90 mA/cm^2) as compared to others (Figure 3b), whereas almost identical response is noticed for the cells in cases (1, 2, 5, 6 and 7) at low applied current density (30 mA/cm^2), as shown in Figure 3a. In general, the cell in case (7) achieves the higher overall battery system among all the studied cases while case (4) represents the worst one.

As the electrode cross section area decreases (Figure 3c), the specific resistance of the electrode will be reduced which, in turn, promotes the electron transfer and enhances the vanadium ions transfer. This ion movement enhancement is attributed to the high inlet velocity in the cell (case 7)

that push and distribute the electrolyte solution in more uniform way, and it can be noticed, more clearly, at high current density conditions where the concentration polarization becomes larger, as depicted in Figure 3b. Overall, it can be concluded that decreasing the cell inlet cross section has a positive effect on the cell voltage response, but there is a limitation for this enhancement depending on the applied operating conditions, i.e., flow rates and current densities.

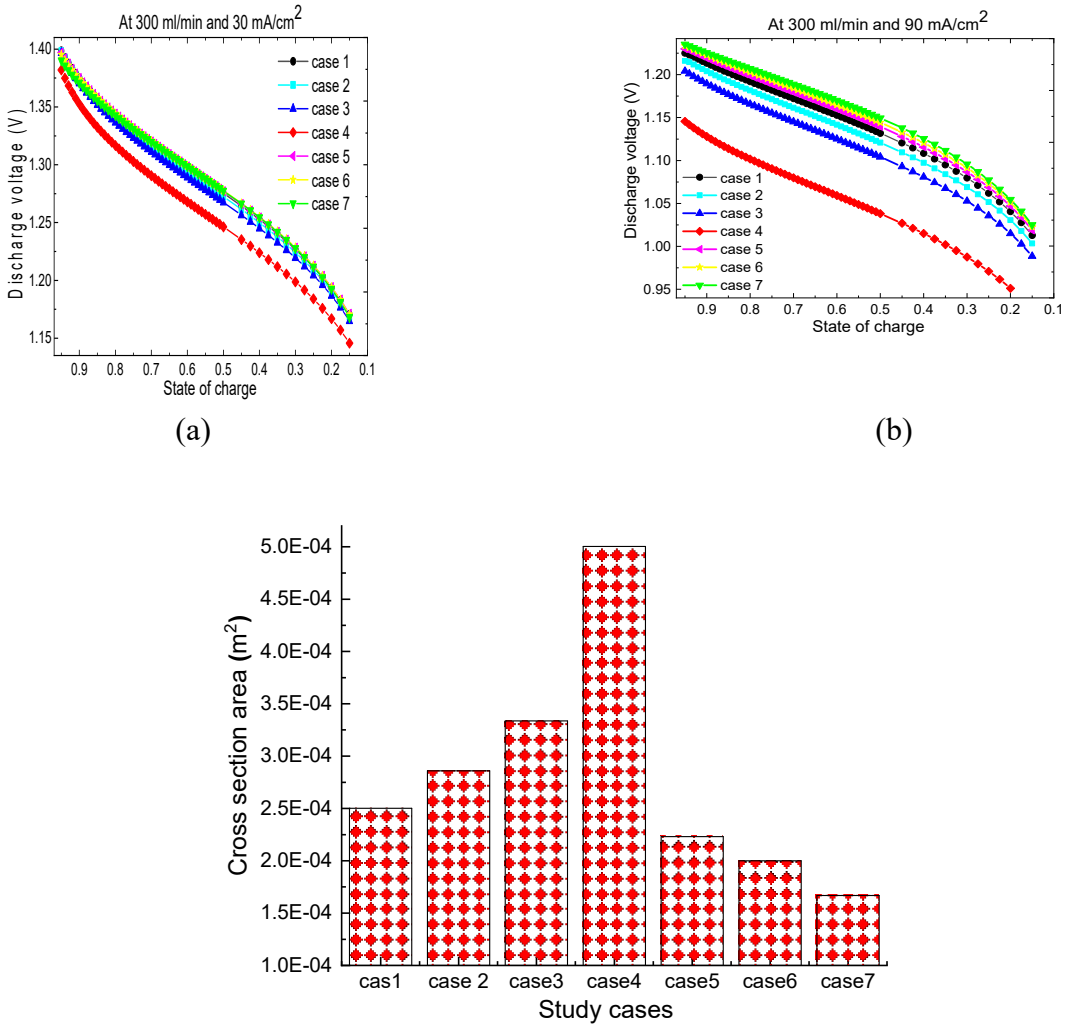

Figure 3. The impact of different electrode configurations on: (a and b) voltage response in a discharge process at (300 ml/min, 30 mA/cm^2) and (300 ml/min, 90 mA/cm^2), respectively, (c) inlet cross section area of electrode.

3.3. Overall battery performance at different cell configurations

Overall battery system efficiency can be, normally, evaluated based on two competitive objectives: concentration overpotential and pumping power [22]. Pumping power is obtained through flow rate and pressure losses according to [19,20]:

$$P_{Pump} = \frac{N_{Pum} \cdot V^{o} \cdot \Delta p}{\eta_{Pum}} \quad (3)$$

where N_{Pum} , V^{o}, η_{Pum}, and Δp represent the number of pumps (two pumps), the actual volumetric flow rate, the pump efficiency (~85%), and the pressure drops average in both electrodes, respectively. Figure 4a,b depict the relation between the pressure drop and correspondence pumping power against range of flow rates for all cases. It is obvious from all cases that a linear behavior is obtained for pressure variation with flow rate, whereas a non-linear relation for pumping power [22]. As it can be seen in Figure 4a,b, higher pressure drop and pumping power in the cell with the smallest cross section area (case 7) due to the high velocity at the electrode inlet cross section area and vice versa for the cell with the largest cross section area (case 4).

Finally, the overall battery efficiency, η_B, is defined as follows [19]:

$$\eta_B = \frac{\int (P_{disch} - P_{pump})\, dSOC}{\int (P_{ch} + P_{pump})\, dSOC} \quad (4)$$

where P_{ch}, P_{disch} are the charging and discharging power, respectively, as a function of SOC. The ratio of input power to output power (P_{ch}/P_{disch}) at 90 mA/cm^2 is shown in Figure 4c. It is obvious that (case 7) has higher output (discharge) power than other cases due to the high discharge voltage response Figure 3b. Two factors are basically controlling the battery efficiency: voltage responses during charging/discharging and pumping losses as indicated in Eq 4. Figure 4d shows the overall battery efficiency with respect to the flow rates for all studied cases at 90 mA/cm^2. It can be seen that (case 7) represents the highest battery efficiency among all cases for the selected range of flow rates in this study. Although the pumping losses is noticed to be higher in (case 7), but the output voltage is improved in a higher ratio, which eventually enhanced the battery efficiency in this case. Therefore, there is a trade-off between these two factors to determine the battery efficiency. It is, also, observed that each cell configuration has its optimal flow rate where the highest battery efficiency can be obtained. The effect of applied current density on battery efficiency has been studied and shown in Table 2. It is noticed, for case 7, that the optimal flow rate is 40 ml/min ($\eta_B = 88.57\%$) at 30 mA/cm^2, while 90 ml/min ($\eta_B = 80.09\%$ and $\eta_B = 73.71\%$) at 60 and 90 mA/cm^2, respectively. Increasing the flow rate behind the optimal value leads to decrease the battery efficiency as pumping power becomes more dominant compared to the small improvement in output voltage responses as indicated in Table 2.

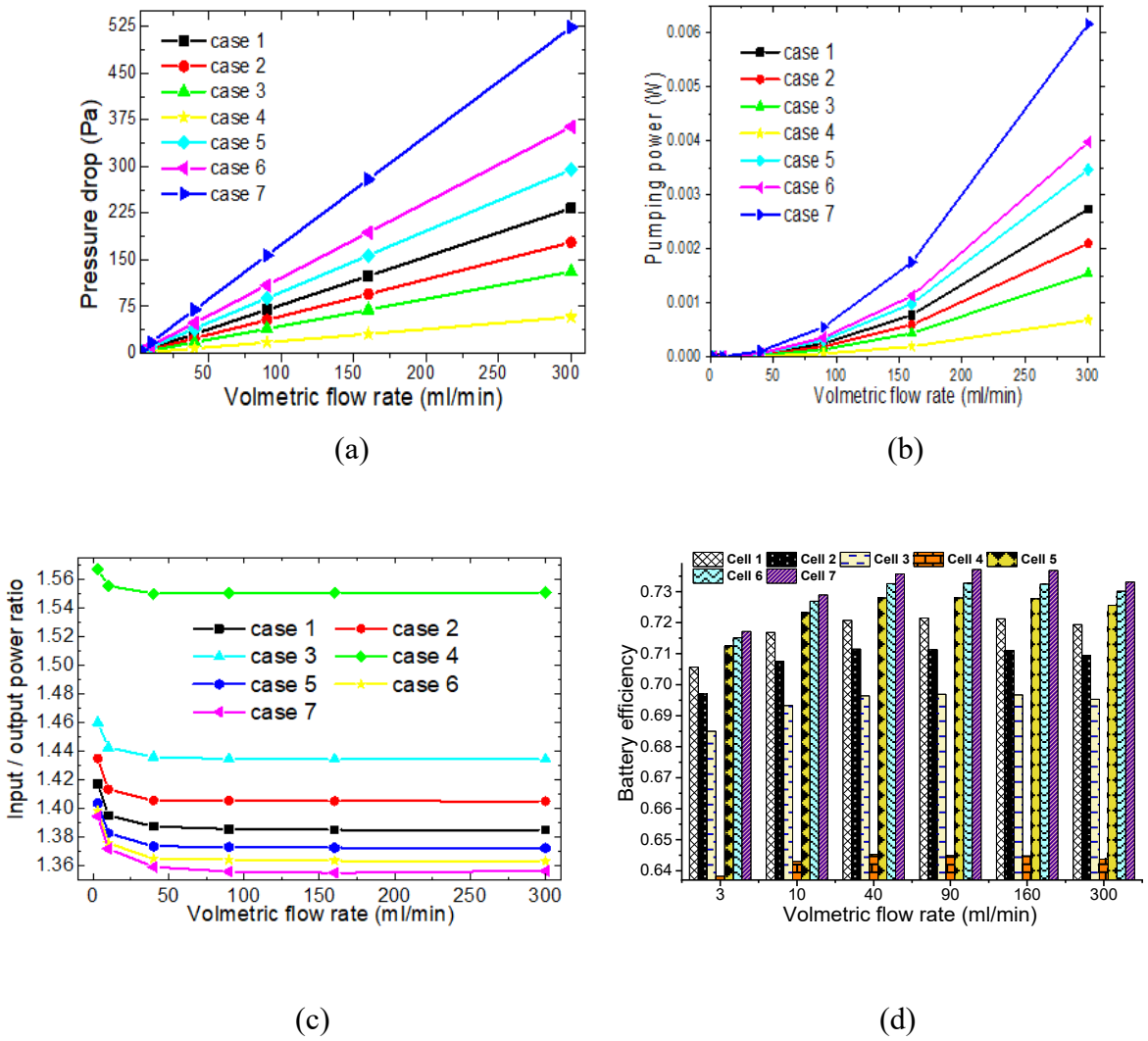

Figure 4. The impact of different electrode configurations on: (a) the pressure drop, (b) the pumping power, (c) the input to output power ratio, (d) the overall battery efficiency at range of flow rates.

Table 2. The overall battery efficiency of 7 cells under various loading conditions.

Cell type	Volumetric flow rate (ml/min)					
	3	10	40	90	160	300
	Current density 30 mA/cm^2					
Cell 1	87.71%	88.35%	88.66%	88.64%	88.46%	87.77%
Cell 2	87.43%	88.10%	88.37%	88.35%	88.20%	87.60%
Cell 3	86.89%	87.61%	87.83%	87.82%	87.68%	87.17%
Cell 4	84.56%	85.18%	85.34%	85.32%	85.24%	84.90%
Cell 5	87.60%	88.42%	88.78%	88.76%	88.56%	87.79%
Cell 6	87.59%	88.38%	88.78%	88.76%	88.54%	87.68%
Cell 7	87.78%	88.45%	88.85%	88.85%	88.69%	87.86%
	Current density 60 mA/cm^2					
Cell 1	77.90%	79.13%	79.40%	79.45%	79.25%	78.95%
Cell 2	77.45%	78.39%	78.73%	78.78%	78.72%	78.45%
Cell 3	76.55%	77.50%	77.64%	77.68%	77.63%	77.40%
Cell 4	72.63%	73.29%	73.45%	73.47%	73.34%	73.20%
Cell 5	78.44%	79.45%	79.79%	79.71%	79.64%	79.30%
Cell 6	78.37%	79.57%	79.98%	80.06%	79.83%	79.46%
Cell 7	78.49%	79.58%	80.01%	80.09%	80.00%	79.65%
	Current density 90 mA/cm^2					
Cell 1	70.57%	71.69%	72.07%	72.15%	72.12%	71.94%
Cell 2	69.70%	70.76%	71.15%	71.13%	71.10%	70.94%
Cell 3	68.50%	69.33%	69.64%	69.69%	69.67%	69.53%
Cell 4	63.82%	64.30%	64.53%	64.49%	64.47%	64.37%
Cell 5	71.25%	72.32%	72.80%	72.80%	72.77%	72.56%
Cell 6	71.51%	72.69%	73.26%	73.27%	73.24%	73.01%
Cell 7	71.72%	72.89%	73.57%	73.71%	73.68%	73.31%

4. Conclusions

Both electrochemistry and fluid mechanic physics have been accounted to develop a 3D numerical model of a single VRFB. The impact of electrode shape on voltage responses, pumping power losses, input to output power ratio, and overall battery efficiency has been studied under various values of operating conditions (flow rates and current densities) as a function of SOCs. Constant electrode volume (10 cm^3) of 7 different configurations has been performed through the numerical model. Results from the simulation show that the configuration of the cell (case 7) has the best battery efficiency under different ranges of flow rates, while the worse one is (case 4) under the same operating conditions. In general, and for all cases, increasing the circulated flow rate can improve the cell voltage response and results in a deeper charge-discharge cycle, however, the pressure losses and the related pumping energy losses increase too. In addition, it is noticed that under different operating conditions, each cell configuration can have various optimal flow rates, where behind this optimal value the battery efficiency decreases. Overall and among all the specified cases in this study, (case 7) has been selected to show better output discharge power and superior battery performance under different operating conditions, on the other side, (case 4) represents the worse cell configuration.

This model can be extended to predict the overpotential and ion vanadium distributions on anode/cathode surfaces, besides the limiting current density.

Conflicts of interest

The author declares no conflict of interest in this paper.

References

1. Dresselhaus M, Thomas I (2001) Alternative energy technologies. *Nature* 414: 332–337.
2. Vanýsek P, Novák V (2017) Redox flow batteries as the means for energy storage. *J Energy Storage* 13: 435–441.
3. Branco H, Castro R, Lopes AS (2018) Battery energy storage systems as a way to integrate renewable energy in small isolated power systems. *Energy Sustainable Dev* 43: 90–99.
4. Ahmed NA, Miyatake M, Al-Othman A (2008) Power fluctuations suppression of stand-alone hybrid generation combining solar photovoltaic/wind turbine and fuel cell systems. *Energy Convers Manage* 49: 2711–2719.
5. Zhao H, Wu Q, Hu S, et al. (2015) Review of energy storage system for wind power integration support. *Appl Energy* 137: 545–553.
6. Sum E, Rychcik M, Skyllas-Kazacos M (1985) Investigation of the V (V)/V (IV) system for use in the positive half-cell of a redox battery. *J Power Sources* 16: 85–95.
7. Skyllas-Kazacos M (1986) New all-vanadium redox flow cell. *J Electrochem Soc* (United States) 133.
8. Schreiber M, Harrer M, Whitehead A, et al. (2012) Practical and commercial issues in the design and manufacture of vanadium flow batteries. *J Power Sources* 206: 483–489.
9. Ferreira HL, Garde R, Fulli G, et al. (2013) Characterisation of electrical energy storage technologies. *Energy* 53: 288–298.
10. Howlader AM, Izumi Y, Uehara A, et al. (2012) A minimal order observer based frequency control strategy for an integrated wind-battery-diesel power system. *Energy* 46: 168–178.
11. Tan CW, Green TC, Hernandez-Aramburo CA (2010) A stochastic method for battery sizing with uninterruptible-power and demand shift capabilities in PV (photovoltaic) systems. *Energy* 35: 5082–5092.
12. Arun P, Banerjee R, Bandyopadhyay S (2008) Optimum sizing of battery-integrated diesel generator for remote electrification through design-space approach. *Energy* 33: 1155–1168.
13. Virulkar V, Aware M, Kolhe M (2011) Integrated battery controller for distributed energy system. *Energy* 36: 2392–2398.
14. Kumar S, Jayanti S (2016) Effect of flow field on the performance of an all-vanadium redox flow battery. *J Power Sources* 307: 782–787.
15. Al-Yasiri M, Park J (2018) A novel cell design of vanadium redox flow batteries for enhancing energy and power performance. *Appl Energy* 222: 530–539.
16. Al-Yasiri M, Park J (2017) Study on channel geometry of all-vanadium redox flow batteries. *J Electrochem Soc* 164: A1970.
17. Chen JQ, Wang BG, Lv HL (2011) Numerical simulation and experiment on the electrolyte flow distribution for all vanadium redox flow battery. *Adv Mater Res*.

18. Al-Yasiri MA (2020) A parametric analysis of the output voltage of all-vanadium redox-flow battery system. *IOP Conference Series: Materials Science and Engineering* 871: 012007.
19. Aaron D, Tang Z, Papandrew AB, et al. (2011) Polarization curve analysis of all-vanadium redox flow batteries. *J Appl Electrochem* 41: 1175.
20. Yin C, Gao Y, Guo S, et al. (2014) A coupled three dimensional model of vanadium redox flow battery for flow field designs. *Energy* 74: 886–895.
21. Shah A, Watt-Smith M, Walsh F (2008) A dynamic performance model for redox-flow batteries involving soluble species. *Electrochim Acta* 53: 8087–8100.
22. Zhang C, Zhao TS, Xu Q, et al. (2015) Effects of operating temperature on the performance of vanadium redox flow batteries. *Appl Energy* 155: 349–353.

AIMS Press